JVI Journals.ASM.org

The Glycoprotein Precursor Gene of Junin Virus Determines the Virulence of the Romero Strain and the Attenuation of the Candid #1 Strain in a Representative Animal Model of Argentine Hemorrhagic Fever

Alexey V. Seregin,[a,b] Nadezhda E. Yun,[a,b,c] Milagros Miller,[a,b] Judith Aronson,[a] Jennifer K. Smith,[a] Aida G. Walker,[a,b] Jeanon N. Smith,[a,b] Cheng Huang,[a,b] John T. Manning,[a,b] Juan C. de la Torre,[d] Slobodan Paessler[a,b,c]

Department of Pathology,[a] Galveston National Laboratory,[b] and Institute for Human Infections and Immunity,[c] University of Texas Medical Branch, Galveston, Texas, USA; Department of Immunology and Microbial Science IMM-6, The Scripps Research Institute, La Jolla, California, USA[d]

ABSTRACT

The New World arenavirus Junin virus (JUNV) is the causative agent of Argentine hemorrhagic fever (AHF), a potentially deadly disease endemic to central regions of Argentina. The live-attenuated Candid #1 (Can) strain of JUNV is currently used to vaccinate the human population at risk. However, the mechanism of attenuation of this strain is still largely unknown. Therefore, the identification and functional characterization of viral genetic determinants dictating JUNV virulence or attenuation would significantly improve the understanding of the mechanisms underlying AHF and facilitate the development of novel, more effective, and safer vaccines. Here, we utilized a reverse genetics approach to generate recombinant JUNV (rJUNV) strains encoding different gene combinations of the pathogenic Romero (Rom) and attenuated Can strains of JUNV. All strains of rJUNV exhibited *in vitro* growth kinetics similar to those of their parental counterparts. Analysis of virulence of the rJUNV in a guinea pig model of lethal infection that closely reproduces the features of AHF identified the envelope glycoproteins (GPs) as the major determinants of pathogenesis and attenuation of JUNV. Accordingly, rJUNV strains expressing the full-length GPs of Rom and Can exhibited virulent and attenuated phenotypes, respectively, in guinea pigs. Mutation F427I in the transmembrane region of JUNV envelope glycoprotein GP2 has been shown to attenuate the neurovirulence of JUNV in suckling mice. We document that in the guinea pig model of AHF, mutation F427I in GP2 is also highly attenuating but insufficient to prevent virus dissemination and development of mild clinical and pathological symptoms, indicating that complete attenuation of JUNV requires additional mutations present in Can glycoprotein precursor (GPC).

IMPORTANCE

Development of antiviral strategies against viral hemorrhagic fevers, including AHF, is one of the top priorities within the Implementation Plan of the U.S. Department of Health and Human Services Public Health Emergency Medical Countermeasures Enterprise. Live-attenuated Candid #1 strain, derived from the 44th mouse brain passage of the prototype XJ strain of JUNV, has been demonstrated to be safe, immunogenic, and highly protective and is currently licensed for human use in Argentina. However, the bases for the attenuated phenotype of Candid #1 have not been established. Therefore, the identification and functional characterization of viral genetic factors implicated in JUNV pathogenesis and attenuation would significantly improve the understanding of the molecular mechanisms underlying AHF and facilitate the development of novel antiviral strategies.

Argentine hemorrhagic fever (AHF), a severe human disease caused by the New World arenavirus Junin virus (JUNV), is clinically characterized by hemorrhagic manifestations and central nervous system (CNS) involvement (1). The incubation period of AHF is usually from 6 to 14 days, followed by the onset of fever with a flu-like syndrome that is considered to be the first day of clinical AHF. Based on the clinical symptoms, the severity of the neurological involvement, and disease outcome, patients are grouped into mild, moderate, and severe clinical forms (2). Patients with severe forms of AHF present with marked CNS manifestations, including areflexia, muscular hypotonia, ataxia, seizures, and coma. Fatal cases are commonly associated with a terminal shock syndrome; superimposed bacterial infections can also be observed (3). Leucopenia and thrombocytopenia are detected during the first and second week after the onset of symptoms. The most frequent hemorrhagic manifestations are petechiae in the mouth and the axillary region and bleeding of the gums. Less common manifestations are epistaxis, hematuria, metrorrhagia, hemoptysis, and gastrointestinal hemorrhages (4). The mortality rates can be up to 30% in cases without specific treatment.

Guinea pigs infected with JUNV reproduce most of the symp-

Received 13 January 2015 **Accepted** 13 March 2015

Accepted manuscript posted online 25 March 2015

Citation Seregin AV, Yun NE, Miller M, Aronson J, Smith JK, Walker AG, Smith JN, Huang C, Manning JT, de la Torre JC, Paessler S. 2015. The glycoprotein precursor gene of Junin virus determines the virulence of the Romero strain and the attenuation of the Candid #1 strain in a representative animal model of Argentine hemorrhagic fever. J Virol 89:5949–5956. doi:10.1128/JVI.00104-15.

Editor: S. Perlman

Address correspondence to Slobodan Paessler, slpaessl@utmb.edu.

doi:10.1128/JVI.00104-15

toms of AHF, including increased viremia from day 7 postinfection (p.i.) until death around day 14 (5), leucopenia and thrombocytopenia, the characteristic hemorrhagic manifestations of AHF, and death, without developing detectable levels of virus-specific antibodies (6, 7). The development of hyperthermia and rapid weight loss are highly predictive of a lethal outcome in infected animals (5). Treatment of JUNV-infected guinea pigs with immune sera may result in the development of a late neurological syndrome with prominent rear-limb paralysis (8). Notably, a late neurological syndrome is also observed in approximately 10% of patients treated with immune plasma from convalescent patients (9, 10).

The arenavirus genome consists of two single-stranded, negative-sense RNA segments, the small (S) and large (L) segments. Each genomic segment uses an ambisense coding strategy to encode two gene products that are expressed in opposite orientations. The L segment (~7 kb) encodes the viral RNA-dependent RNA polymerase (LP) and a small RING finger protein (Z) that has the properties of a bona fide matrix protein found in many enveloped negative-strand RNA viruses. The S segment (~3.4 kb) encodes the glycoprotein precursor (GPC) and the nucleoprotein (NP). GPC is co- and posttranslationally processed by signal peptidase and SKI-1/S1P cellular proteases, respectively, to yield two glycoproteins, GP1 and GP2, and the stable signal peptide (SSP) that form GP1/GP2/SSP glycoprotein complexes on the surface of mature virions and mediate virion attachment and cell entry. NP is the most abundantly present viral protein in both infected cells and virions. NP is the main structural component of the arenavirus ribonucleoprotein (RNP) core that directs both replication and transcription of the virus genome (11).

As with many other viruses, arenaviruses have evolved mechanisms to modulate the host cell responses to infection. Thus, NP has been shown to exhibit a type I interferon (IFN-I) counteracting activity (12–14). This function of NP was mapped to its C terminus and linked to the DEDDH 3′–5′ exonuclease domain present within the C-terminal part of NP (15, 16). Likewise, the Z protein of the New World pathogenic arenaviruses has been shown to interfere with induction of IFN-I mediated by the cytosolic pattern recognition receptor RIG-I. In addition, Z was found to interact with a variety of cellular factors, including the promyelocytic leukemia (PML) protein, which has been proposed to contribute to the noncytolytic nature of the prototypic arenavirus lymphocytic choriomeningitis virus (LCMV) (17, 18). Z has also been shown to bind eukaryotic translation initiation factor 4E (eIF4E) (19, 20), which can result in translation inhibition of selected cellular mRNAs, including transcription factor IRF7 required for IFN-I production by plasmocytoid dendritic cells.

The identification and characterization of the viral determinants contributing to the virulence and pathogenesis of JUNV remain largely unknown, but evidence suggests a contribution of the viral GPs (21, 22). Thus, only GPs from pathogenic New World arenaviruses, including JUNV, use human transferrin receptor 1 (TfR1) as the primary receptor for cell entry (23), whereas nonpathogenic New World arenaviruses appear to enter human cells via TfR1-independent pathways. Nevertheless, pathogenic New World arenaviruses can also infect cells via TfR1-independent pathways, albeit less efficiently (24). Interestingly, the F427I substitution found in the transmembrane region of GP2 of the attenuated Candid #1 (Can) strain of JUNV was shown to significantly attenuate the parental pathogenic virus in suckling mice inoculated intracranially (21). Further analysis revealed that this mutation was responsible for decreased infectivity of Can in human cells (22). However, the suckling-mouse-neurovirulence model does not accurately reproduce the pathobiological features of human AHF, while immunocompetent adult laboratory mice are highly resistant to challenge with JUNV and rapidly clear the infection regardless of the inoculation route. Therefore, studies in more-relevant animal models, guinea pigs and nonhuman primates, addressing the role of the F427I mutation in *in vivo* attenuation of JUNV are needed. Here, we describe the generation of recombinant viruses where either the entire RNA segments or individual viral genes were exchanged between the attenuated Can and the pathogenic Romero (Rom) strains of JUNV. Analysis of the *in vitro* growth properties of these viruses demonstrated that all viral proteins exhibited a high degree of compatibility between the two viral strains. Analysis of the *in vivo* biological properties of the chimeric JUNVs revealed that GPC is a main determinant of the pathogenicity and virulence of Rom and the attenuation of Can. Importantly, mutation F427I in the GP2 that attenuated the neurovirulence of JUNV in suckling mice also significantly attenuated Rom in a guinea pig model of lethal infection. However, this mutation was not sufficient to prevent disease development and additional mutations present in the GPC of Can were required for complete *in vivo* attenuation of the virus.

MATERIALS AND METHODS

Cells, viruses, and biosafety. Baby hamster kidney (BHK-21) and Vero cells (American Tissue Culture Collection) were maintained in Dulbecco's modified Eagle's medium supplemented with 10% fetal calf serum and L-glutamine. Viral stocks were prepared by infecting Vero cells (multiplicity of infection [MOI] = 0.01) and collecting virus-containing tissue culture supernatants (TCS) at 4 days postinfection (p.i.), followed by elimination of cell debris by centrifugation (10,000 × *g* for 10 min at 4°C). Work with virulent strains of JUNV and animal experiments were performed in the University of Texas Medical Branch (UTMB) biosafety level 4 (BSL-4) facilities in accordance with institutional health and safety guidelines.

Rescue of chimeric JUNV variants. Generation of RNA polymerase I/II (pol-I/II) reverse genetics systems for Romero and Candid #1 and rescue of recombinant Romero (rRom) and recombinant Candid #1 (rCan) viruses have previously been described (25). Plasmids mPol-I-Sag and mPol-I-Lag carrying recombinant S and L segments, respectively, in antigenomic orientation were generated by genetically engineering the open reading frames (ORF) of Candid #1 genes into the Romero genome. Recombinant JUNV (rJUNV) was rescued in BHK21 cells as described for rRom and rCan (25) by transfection with the corresponding mPol-I-Sag and mPol-I-Lag plasmids together with pol-II plasmids pC-NP and pC-LP expressing the NP (pC-NP) and L polymerase (pC-LP) of Rom.

Virus propagation, growth kinetics, and titration. Virus growth kinetics in cultured cells were assessed by infecting Vero cells (MOI = 0.1 or 5) and collecting TCS at the indicated times. Virus titers in TCS were determined by a plaque assay. Briefly, 10-fold dilutions of TCS specimens were added to Vero cell monolayers in twelve-well culture plates for 1 h at 37°C in an atmosphere of 5% CO_2 and were then overlaid with minimum essential medium (MEM) containing 5% fetal bovine serum, 1% penicillin-streptomycin (P/E) solution, and 0.5% agarose. Plates were then incubated for 6 days at 37°C, and plaques were revealed by fixation of cell monolayers with formaldehyde, followed by crystal violet staining. Infected tissues were dissected at necropsy and homogenized in MEM containing 1% P/E. Homogenates were clarified by centrifugation, and the supernatants were used for plaque assays as described for TCS specimens.

Animal experiments. Ten-week-old female Hartley guinea pigs were purchased from The Charles River Laboratory and housed for at least 7

days in a specific-pathogen-free environment before being used in any experimental procedure. All animal studies were reviewed and approved by the Institutional Animal Care and Use Committee at the UTMB and were carried out according to the National Institutes of Health guidelines under BSL-4 conditions. Guinea pigs were anesthetized using an isoflurane precision variable-bypass vaporizer prior to virus inoculation by the intraperitoneal (i.p.) route with 10^3 PFU. Standardized recording of death and disease symptoms was performed using the following definitions: encephalitis, development of discoordination, ataxia, or transient seizures (with the ability to drink and feed); paralysis, hind limb (hemiplegic) or quadriplegic paralysis (with the inability to reach the feeder or water bottle). Telemetric monitoring of body temperature and measurement of body weight were performed during the course of study. For telemetry, animals were anesthetized and implanted subcutaneously with BMDS IPTT-300 transponders (chips) obtained from Bio Medic Data Systems, Inc. (Seaford, DE), using a trocar needle assembly. Animals were monitored for signs of infection or transponder migration for 2 days prior to transfer to the BSL-4 facility. Chips were scanned using a DAS-6007 transponder reader (Bio Medic Data Systems, Inc.). Downloading of digital temperature data was performed in accordance with the manufacturer's protocol.

Hematological and clinical chemical analyses. Blood from guinea pigs was collected into tubes containing EDTA, and a standard hematologic analysis was performed using a Hemavet 1700 analyzer (Drew Scientific, Inc.) and whole-blood specimens to determine platelet and differential counts, in accordance with the manufacturer's recommendation. Clinical chemical analysis was performed using VetScan VS2 and the comprehensive diagnostic profile (Abaxis) according to the manufacturer's instructions.

Histopathological analysis. Tissue samples were fixed in 4% buffered formalin for a minimum of 7 days and stored in 70% ethanol for 12 h. The samples were then embedded in paraffin. Tissue sections (4 μm in thickness) were mounted on slides and subjected to standard hematoxylin and eosin (H&E) staining as described previously (25).

PRNT. Plaque reduction neutralization tests (PRNT) were performed on Vero monolayers. Briefly, 40 PFU of Candid #1 was incubated for 1 h at 37°C with 2-fold dilutions of serum samples taken from guinea pigs infected with chimeric viruses. Subsequently, cell monolayers were incubated with virus-serum mixtures for 1 h at 37°C, overlaid with 0.5% agarose, maintained for 6 days at 37°C, and stained with crystal violet. The serum dilutions corresponding to an endpoint of 50% plaque reduction were determined.

Quantitative real-time PCR. Total RNA from infected tissues lysed in TRIzol reagent (Invitrogen) was isolated using a Direct-zol RNA MiniPrep kit (Zymo Research) following the manufacturer's protocol. Viral RNA quantification was performed in triplicate using a iScript One-Step reverse transcription-PCR (RT-PCR) kit with SYBR green (Bio-Rad) and 100 ng of total RNA. The following primers were used for detection: NP forward, GGTCCTTCAATGTCGAGCCA; NP reverse, AATCACAGGCA GGTCATGGG; Z forward, AAGTGCTGCTGGTTTGCTGA; Z reverse, TCCACCGGTACTGTGATTGTG; GAPDH (glyceraldehyde-3-phosphate dehydrogenase)-Vero forward, AGTCAACGGATTTGTCGTA; GAPDH-Vero reverse, GGGTGGAATCATACTGGAAC; GAPDH-guinea pig forward, TACGACAAGTCCCTCAAGATTG; GAPDH-guinea pig reverse, TCTGGGTGGCAGTGATGG. Melt curve analysis was performed to confirm PCR fragment specificity. Sample cycle threshold (C_T) values were normalized to the C_T values of GAPDH. Relative amounts of viral RNA in infected cells and tissues were calculated against rRomero RNA using $2^{-\Delta CT}$, where $\Delta C_{T\text{sample}} = (C_{T\text{sample}} - C_{T\text{GAPDH/sample}}) - (C_{T\text{rRomero}} - C_{T\text{GAPDH/rRomero}})$ (26).

RESULTS

Rescue and *in vitro* growth properties of inter- and intrasegment chimeric viruses in genetic exchanges between the Romero (Rom) and Candid #1 (Can) strains of JUNV. The highly pathogenic Rom strain and attenuated Can strain of JUNV exhibit significant differences in amino acid sequences of the viral proteins (8, 7, 2, and 49 amino acid [aa] changes in the GPC, NP, Z, and LP loci, respectively) (25). We have documented that the polymerase complexes of Rom and Can replicate and transcribe the S segment of Can with similar efficiencies (25). This observation led us to consider the feasibility of using reverse genetic approaches to rescue rJUNV with genetic information exchanged between the Rom and Can strains of JUNV. Accordingly, we rescued viruses that had one genome RNA segment from Rom and the other segment from Can (rRomL/CanS and rCanL/RomS) (Fig. 1A). We then compared the efficiency of plaque formation of these chimeric rJUNV strains in Vero cells with that of rRom and rCan. We found that rCanL/RomS produced large plaques that were similar in size and morphological appearance to those of rRom (Fig. 1B). In contrast, rRomL/CanS produced small plaques similar to those of Can (Fig. 1B). These results suggested that the genetic determinants of the JUNV plaque phenotype are encoded by the S genome segment. To determine which viral gene carried by the S segment was responsible for the plaque phenotype observed for the reassortant rJUNV, we rescued two rJUNV strains that expressed the GPC gene (rRom/CanGPC) or NP gene (rRom/CanNP) of Can in the backbone of the Rom genome (Fig. 1A). Both rRom/CanGPC and rRom/CanNP produced plaques on Vero cells that were of a size intermediate between those of Rom and Can (Fig. 1B). This result indicated that both viral genes carried by the S segment contribute to the JUNV plaque phenotype.

Next, we investigated whether the observed small and medium-size plaque phenotypes correlated with impaired growth capacity of the corresponding rJUNV in cultured cells. For this, we infected (MOI = 5) IFN-deficient (Vero) and IFN-competent (A549) cells and determined titers of infectious virus in tissue culture supernatants (TCS) over time to examine the one-step growth curve for each rJUNV strain and compared them to those of the parental rRom and rCan. All rescued rJUNV strains and the corresponding parental rRom and rCan strains exhibited similar growth kinetics in both Vero and A549 cells (Fig. 1D). These results indicated that the observed differences in plaque phenotype did not reflect impaired growth properties in cultured cells.

Recently, a single amino acid substitution in the transmembrane region of GP2 (F427I) of the XJ13 strain of JUNV, which is a guinea pig-attenuated but mouse-neurovirulent strain, was shown to further increase attenuation in suckling mice and was proposed to be a major attenuating mutation of Can (21). To further evaluate the phenotypic manifestations of the GP2 F427I mutation in cultured cells, we used the reverse genetics approach to generate rRom/G2/F427I, in which the phenylalanine at position 427 of the GPC was replaced by isoleucine (F427I). The rescued rRom/G2/F427I strain exhibited growth properties in Vero and A549 cells similar to those displayed by rRom and rCan (Fig. 1C and D). Interestingly, rRom/G2/F427I produced large plaques in Vero cells that were similar in size and morphology to those of rRom (Fig. 1B), indicating that the F427I substitution in the GPC of Candid #1 was not responsible for the small-plaque phenotype exhibited by Can.

***In vivo* biological properties of inter- and intrasegment chimeric viruses.** The neurovirulence of JUNV in suckling mice has been associated with the viral GPC (21). However, the viral genetic determinants of JUNV pathogenesis and virulence in outbred Hartley guinea pigs, a well-established animal model of human

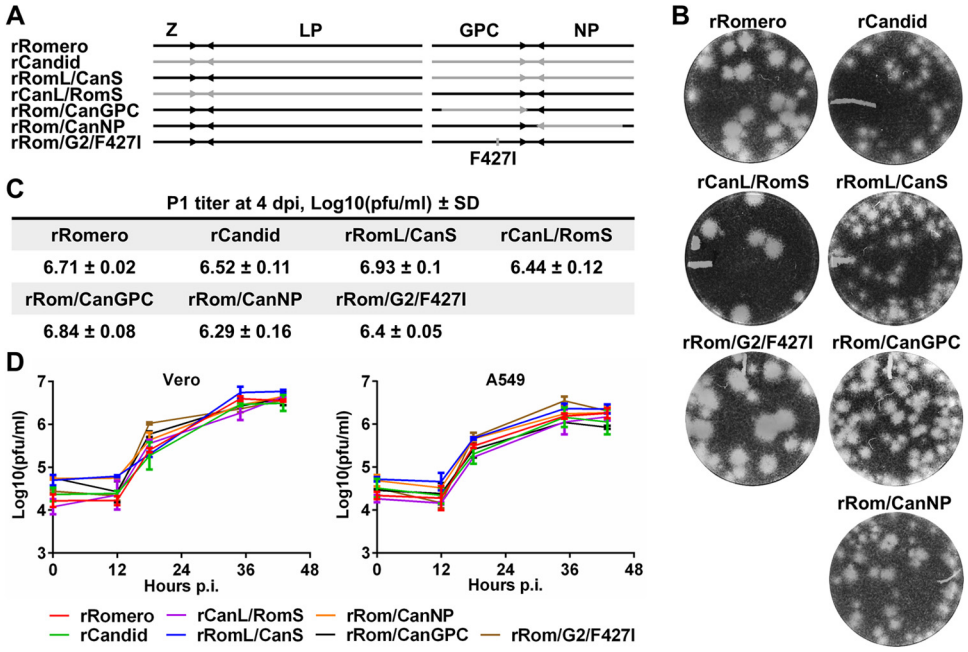

FIG 1 Rescue and characterization of rJUNV with inter- and intrasegment rearrangements between the Rom and Can strains of JUNV. (A) Schematic representation of rJUNV genomes. Black and gray colors indicate the genetic material of Rom and Can strains of JUNV, respectively. (B) Plaque phenotype on Vero cells. Infected cell monolayers were overlaid with growth medium containing 0.5% agarose and incubated for 7 days. Cells were stained with crystal violet to visualize plaques. (C) Passage 1 (P1) titers on Vero cells were determined by plaque assay at 4 days p.i. (dpi). (D) One-step growth curves of rJUNVs on Vero (left) and A549 (right) cells. TCS of cells infected at an MOI of 5 were collected at the indicated times, and titers were determined by plaque assay.

AHF (25), have not been determined. To investigate this issue, we infected (i.p., 10^3 PFU) Hartley guinea pigs with rRomL/CanS, rCanL/RomS, or rRom/G2/F427I (Fig. 1A) and monitored their survival and disease manifestations compared to those of guinea pigs infected with the parental viruses, rRom and rCan (Fig. 1A). Guinea pigs infected with rCanL/RomS or with rRom experienced a steady weight loss starting at 7 days p.i. that was followed by rapid deterioration of the health of the animals around 11 days p.i., with development of fever, rapid weight loss, and uniformly lethal outcome between days 17 and 19 p.i. (Fig. 2). In contrast, none of the guinea pigs inoculated with rRomL/CanS developed any clinical symptoms (Fig. 2A) and all infected animals gained weight during the observation period (Fig. 2C). Likewise, the body temperature of these animals stayed within the normal range (37 to 39.7°C) throughout the course of the experiment (Fig. 2B). Interestingly, all guinea pigs inoculated with rRom/G2/F427I survived the infection (Fig. 2A). However, two of three experimental animals experienced mild weight loss between days 4 and 8 p.i. (Fig. 2C); one of them also developed a transient fever that fully resolved by day 10 p.i. (Fig. 2B). Analysis of the clinical hematology and blood chemistry parameters of the infected guinea pigs revealed that infection with rCanL/RomS, similarly to rRom infection, caused thrombocytopenia and general immunosuppression indicated by the reduction of platelet, lymphocyte, and total white blood cell counts, as well as by the decrease in albumin production and release of liver enzymes, most likely associated with liver damage (Table 1). In contrast, the hematological and blood chemistry values of rRom/CanS- and rRom/G2/F427I-infected animals were very similar to those of rCan-infected animals (Table 1).

To further evaluate and compare the degrees of *in vivo* attenuation seen with strains rRomL/CanS and rRom/G2/F427I, we determined the kinetics of serum neutralizing antibody production by the PRNT assay using rCan as the test virus. Infection with rRomL/CanS induced neutralizing antibody titers (Fig. 3) comparable to those previously published for rCan-infected guinea pigs (25). Interestingly, rRom/G2/F427I infection induced much higher neutralizing antibody titers at 30 and 45 days p.i. than rRomL/CanS infection (Fig. 3).

These findings indicated that the S segment encodes critical determinants of JUNV virulence and attenuation in guinea pigs. Moreover, consistent with results from a study using a mouse model of JUNV neurovirulence (21), mutation F427I in the transmembrane domain of GP2 significantly attenuated Rom in outbreed Hartley guinea pigs, but additional mutations present in the S segment of Can were required for complete attenuation of the virus.

To investigate the individual contributions of the S segment-encoded NP and GPC gene products to the attenuation of JUNV in the guinea pig model of AHF, we used rRom/CanNP or rRom/CanGPC (Fig. 1) to infect guinea pigs and monitored them over time (Fig. 4). All animals infected with rRom/CanNP developed disease symptoms characteristic of Rom infection, accompanied with fever (Fig. 4B) and weight loss (Fig. 4C), and succumbed to infection by 20 days p.i. (Fig. 4A). In contrast, all guinea pigs infected with rRom/CanGPC survived (Fig. 4A) without exhibiting any detectable disease symptoms (Fig. 4B). These data demonstrated that the amino acid changes accumulated in the GPC during *in vivo* and *in vitro* passages of JUNV to generate the Candid #1 vaccine strain are the main determinants of the attenuated phenotype of Candid #1 in guinea pigs.

To confirm that complete attenuation of rJUNV in guinea pigs

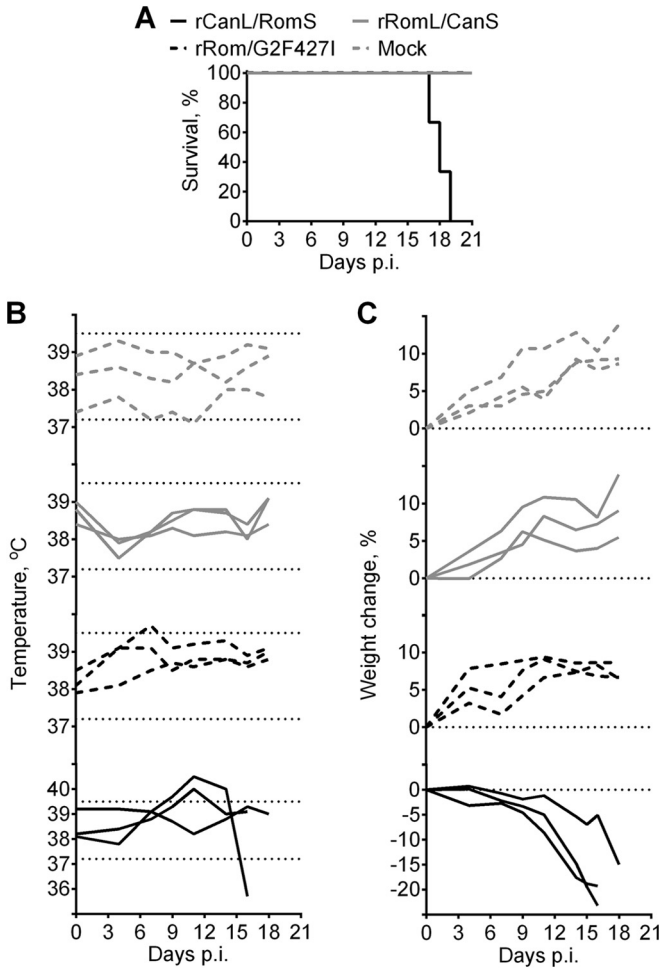

FIG 2 Survival and disease manifestations in guinea pigs infected with rRomL/CanS, rCanL/RomS, and rRom expressing the F427I mutation in GP2 (rRom/G2F427I). (A) Hartley guinea pigs were inoculated i.p. with 10^3 PFU of rJUNVs ($n = 3$) and monitored for 21 days for survival. (B and C) Body temperature changes (B) and weight changes (C) were recorded throughout the course of the study. The range of normal guinea pig body temperature (37.2 to 39.5°C) is flanked by dashed lines on temperature graphs.

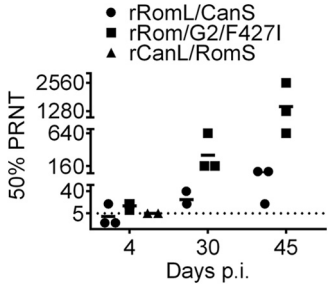

FIG 3 Imunogenicity comparison between rRomL/CanS, rCanL/RomS, and rRom/G2F427I. Serum samples were collected from infected guinea pigs at the indicated time points, and the titers of Candid #1-specific neutralizing antibodies were determined by 50% plaque reduction neutralization tests (PRNT). The horizontal dotted line indicates average titer values.

was achieved only when the clones expressed the full-length GPC of Candid #1 origin, we compared histopathological manifestations in the spleen and liver of guinea pigs infected with the different rJUNV strains: rRomL/CanS, rCanL/RomS, rRom/CanNP rRom/CanGPC, rRom/G2/F427I, and parental viruses rRom and rCan. We selected these organs because they have been shown to exhibit the most pronounced pathological changes in Rom-infected guinea pigs (25). We prepared histological sections from three animals randomly selected in each group that were euthanized at 11 days p.i. Following hematoxylin and eosin staining, sections were evaluated by a pathologist in a blind manner with respect to the conditions of the experiment (Table 2). All animals infected with rCanL/RomS or rRom/CanNP, all of which succumbed to infection, exhibited histopathological changes very similar to those found in the organs of rRom-infected animals. The changes in the spleen were characterized by congestion and decreased cellularity of the red pulp, the presence of macrophages and scattered polymorphonuclear cells, and depletion of the white pulp without overt necrosis. The manifestations in the liver were characterized by diffuse microvesicular and, sometimes, macrovesicular steatosis, periportal and lobular inflammation, and the presence of nuclear debris in portal triads. In general, the spleen and liver of guinea pigs infected with rRomL/CanS, rRom/CanGPC, or rRom/G2/F427I did not show any (or showed minimal) significant pathological changes; however, occasionally, rare foci of periportal and lobular inflammation were observed in the liver and the presence of scattered macrophages was detected in the white pulp of the spleen. Intriguingly, the histopathological manifestations in the organs of rRom/G2/F427I-infected guinea pigs were more pronounced than the changes observed in the organs of rRomL/CanS- or rRom/CanGPC-infected animals. Specifically, the livers of guinea pigs infected with rRom/G2/F427I showed more foci of mononuclear cell inflammation with the

TABLE 1 Hematology and blood chemistry parameters in guinea pigs infected with virulent and attenuated chimeric JUNV variants

Group[b]	Preinoculation/postinoculation values[a]				
	Platelet count (10^3/ml)	White blood cell count (k/μl)	Lymphocyte count (k/μl)	Albumin (g/dl)	Alanine aminotransferase (U/liter)
rRomero	463 ± 122/40 ± 15	5.86 ± 1.7/1.82 ± 0.91	3.69 ± 0.76/0.75 ± 0.37	4.0 ± 0.1/3.0 ± 1.1	34 ± 9/79 ± 25
rCanL/RomS	465 ± 109/137 ± 70	4.79 ± 1.23/1.81 ± 0.56	3.33 ± 0.29/0.62 ± 0.24	4.1 ± 0.3/2.3 ± 0.1	30 ± 3/52 ± 15
rRom/CanNP	518 ± 188/164 ± 74	4.53 ± 0.79/1.87 ± 1.0	3.15 ± 0.29/0.62 ± 0.07	4.1 ± 0.3/2.3 ± 0.4	28 ± 1/46 ± 9
rCandid #1	447 ± 110/464 ± 190	5.60 ± 1.5/6.14 ± 1.64	3.73 ± 1.22/4.48 ± 1.07	3.8 ± 0.0/4.0 ± 0.3	27 ± 6/33 ± 10
rRomL/CanS	493 ± 165/484 ± 124	5.29 ± 0.88/7.44 ± 1.61	3.38 ± 0.47/5.34 ± 1.89	4.2 ± 0.5/3.8 ± 0.4	30 ± 7/29 ± 8
rRom/CanGPC	447 ± 53/590 ± 103	5.01 ± 0.67/9.22 ± 4.17	3.22 ± 0.72/4.01 ± 1.14	4.6 ± 0.6/3.9 ± 0.2	30 ± 4/34 ± 6
rRom/G2/F427I	544 ± 107/528 ± 101	3.96 ± 0.6/6.41 ± 2.3	2.75 ± 0.64/4.81 ± 1.68	4.1 ± 0.2/3.8 ± 0.3	29 ± 5/32 ± 2

[a] Blood was collected preinfection (day −7) and postinfection (day +12), and hematology and blood chemistry parameters were analyzed.
[b] Hartley guinea pigs were inoculated i.p. with 10^3 PFU of rJUNVs.

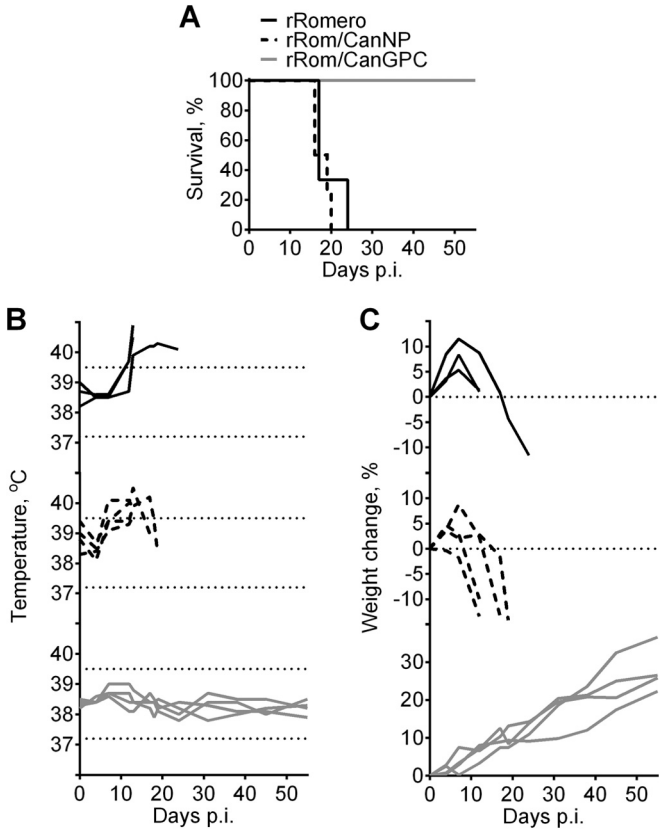

FIG 4 Comparisons of survival and disease characteristics of guinea pigs infected with intra-S segment rJUNV between the Rom and Can strains of JUNV. (A) Hartley guinea pigs were inoculated i.p. with 10^3 PFU of rJUNVs and monitored for 50 days for survival. (B and C) Body temperature changes (B) and weight changes (C) were recorded throughout the course of the study. The range of normal guinea pig body temperature (37.2 to 39.5°C) is flanked by dashed lines on temperature graphs.

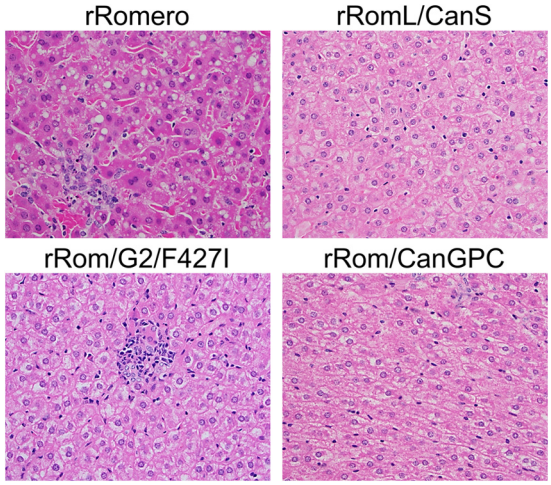

FIG 5 Liver histopathology in guinea pigs infected with chimeric JUNV variants. Tissue sections from infected guinea pigs were subjected to standard H&E staining. ×40 magnification is shown.

presence of hepatocyte apoptosis (Fig. 5). These results would suggest that rRom/G2/F427I replicates more efficiently in the organs of infected guinea pigs than rRomL/CanS and rRom/CanGPC. To further examine the possible greater organ distribution of rRom/G2/F427I, compared to rRomL/CanS and rRom/CanGPC, we determined levels of viral RNA in the brain, spleen, and liver at 11 days p.i. Although infectious virus could not be detected in the spleen or liver of infected animals in any of the experimental groups, rRom/G2/F427I-infected animals contained greater amounts of viral RNA in the brain than rRomL/CanS- and rRom/CanGPC-infected animals (Fig. 6). Of note, the presence of the F427I mutation in the RNA of rRom/G2/F427I isolated from the brain of infected guinea pigs was confirmed by sequencing (data not shown). These results identified mutation F427I as one that significantly contributed to attenuation of JUNV in guinea pigs, but additional mutations in Can GPC were required to restrict viral replication in the organs of infected animals to below pathogenic levels.

DISCUSSION

Here, we have described the use of reverse genetic approaches to rescue rJUNV by exchanges between the highly pathogenic Rom strain and the attenuated Can strain of JUNV. For this, we used a pol-I/II reverse genetics system that we have previously described (25). To rescue rJUNV, we either exchanged the L and S genome RNA segments between Rom and Can or substituted individually the GPC and NP genes carried by the S segment of Can for the corresponding counterpart in the genome of Rom (Fig. 1A).

Analysis of the *in vitro* growth properties of the different rJUNV strains showed that the GPC/NP and Z/LP combinations encoded by the S and L segments, respectively, were fully exchangeable between the Rom and Can strains, as both the rRomL/CanS and rCanL/RomS viruses exhibited growth kinetics similar to those of the parental rRom and rCan viruses in both IFN-I-deficient (Vero) and IFN-I-competent (A549) cell lines (Fig. 1C).

TABLE 2 Histopathological findings in tissues of guinea pigs infected with chimeric JUNV variants

Virus group[a]	Virulence for guinea pigs	Histological change(s)[b]	
		Spleen	Liver
rRomero, rCanL/RomS, rRom/CanNP	Yes	Congested and depleted red pulp; depleted, nonreactive white pulp; scattered macrophages and polymorphonuclear cells	Microvesicular and macrovesicular steatosis; periportal and lobular inflammation
rCandid #1, rRomL/CanS, rRom/CanGPC, rRom/G2/F427I	No	Unremarkable	Rare foci of periportal and lobular inflammation

[a] Guinea pigs were inoculated i.p. with 10^3 PFU of rJUNVs and euthanized at 12 days p.i. (dpi).
[b] Histopathologic analysis was performed on H&E-stained tissue sections.

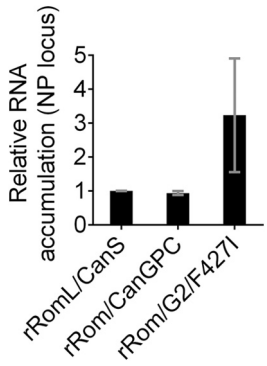

FIG 6 Levels of viral RNA in brains of infected guinea pigs. Total RNA was extracted from brain tissues of rJUNV-infected guinea pigs euthanized at 12 days p.i. Quantitative RT-PCR using SYBR green dye was performed in triplicate. Levels of RNA derived from the NP locus were normalized to GAPDH mRNA levels and expressed as ratios relative to the NP RNA level in rRomL/CanS brain tissue sample. Average values and standard deviations are shown.

Plaque phenotypes of rJUNV were determined by the origin of the S segment; rCanL/RomS produced large plaques similar to those produced by rRom, whereas rRomL/CanS produced small plaques similar to those produced by rCan (Fig. 1B). Our finding that rRom/CanGPC and rRom/CanNP exhibited growth kinetics in both Vero and A549 cells that were similar to those observed for rRom and rCan (Fig. 1D) indicated that Can GPC and NP could substitute for the Rom counterparts very efficiently. Interestingly, both rRom/CanNP and rRom/CanGPC produced plaques of a size intermediate between those produced by rRom and rCan, indicating that both NP and GPC contributed to the plaque phenotype. The small-plaque phenotype of rCan and rJUNV containing genes carried by the S segment of Can could reflect that these viruses are more potent apoptosis inducers than rRom, which could lead to early cell death and limited cell-to-cell viral spread under conditions of agarose overlay. However, the exact mechanism of this process requires further investigation. Mutation F427I in the GP2 that has been shown to increase attenuation of XJ13 strain in suckling mice (21) neither affected the growth kinetics nor changed the plaque phenotype of rRom (Fig. 1B). Together, these results demonstrated that the plaque phenotype of the different rJUNV strains does not correlate with their ability to replicate and produce infectious progeny in cultured cells.

All the rJUNV strains that we rescued and tested in this study could be divided into two groups based on their virulence, pathogenicity, and clinical disease parameters in guinea pigs: the Rom-like viruses and the Can-like viruses. All viruses that encoded the GPC derived from Rom (rRomero, rCanL/RomS, and rRom/CanNP) exhibited a virulent phenotype in guinea pigs, demonstrating that GPC is a major determinant of JUNV virulence in a validated animal model of human AHF. In contrast, the rJUNV strains that encoded the GPC of Candid #1 (rCandid, rRomL/CanS, and rRom/CanGPC), or the GPC of Romero containing the F427I mutation in GP2 (rRom/G2/F427I), were highly attenuated in guinea pigs (Fig. 2A and 4A). Nevertheless, animals infected with rRom/G2/F427I developed mild, nonlethal disease that fully resolved by the end of observation period (Fig. 2). Notably, rRom/G2/F427I-infected guinea pigs developed much higher neutralizing antibody titers than rRomL/CanS-infected guinea pigs (Fig. 3) and also had greater amounts of viral RNA in the brain than guinea pigs infected with either rRomL/CanS or rRom/CanGPC (Fig. 6). This likely reflected a better ability of rRom/G2/F427I to replicate in the tissues of infected guinea pigs. This hypothesis was further supported by histological analysis of tissue sections from infected guinea pigs, which revealed higher levels of immune cell infiltration in the organs of the rRom/G2/F427I-infected animals than in the rRomL/CanS- and rRom/CanGPC-infected animals (Table 2 and Fig. 5). Our findings support the conclusion that mutation F427I in the transmembrane region of G2 is sufficient to cause high levels of JUNV attenuation but that it does not prevent virus dissemination and development of mild clinical and pathological symptoms. Therefore, complete attenuation of JUNV requires additional mutations present in Can GPC.

ACKNOWLEDGMENTS

A.V.S. was supported by Biodefense Training Program, NIH, grant T32-AI060549. This work was supported by Public Health Service grant R01AI093445 to S.P. and J.C.D.L.T.

REFERENCES

1. **Elsner B, Schwarz E, Mando OG, Maiztegui J, Vilches A.** 1973. Pathology of 12 fatal cases of Argentine hemorrhagic fever. Am J Trop Med Hyg **22:**229–236.
2. **Molinas FC, Kordich L, Porterie P, Lerer G, Maiztegui JI.** 1987. Plasminogen abnormalities in patients with argentine hemorrhagic fever. Thrombosis Res **48:**713–720. http://dx.doi.org/10.1016/0049-3848(87)90436-1.
3. **Marta RF, Montero VS, Molinas FC.** 1998. Systemic disorders in Argentine haemorrhagic fever. Bulletin de l'Institut Pasteur **96:**115–124.
4. **Molinas FC, de Bracco MME, Maiztegui JI.** 1981. Coagulation studies in Argentine hemorrhagic fever. J Infect Dis **143:**1–6. http://dx.doi.org/10.1093/infdis/143.1.1.
5. **Yun NE, Linde NS, Dziuba N, Zacks MA, Smith JN, Smith JK, Aronson JF, Chumakova OV, Lander HM, Peters CJ, Paessler S.** 2008. Pathogenesis of XJ and Romero strains of Junin virus in two strains of guinea pigs. Am J Trop Med Hyg **79:**275–282.
6. **Enria DA, Briggiler AM, Sánchez Z.** 2008. Treatment of Argentine hemorrhagic fever. Antiviral Res **78:**132–139. http://dx.doi.org/10.1016/j.antiviral.2007.10.010.
7. **Laguens RM, Avila MM, Samoilovich SR, Weissenbacher MC, Laguens RP.** 1983. Pathogenicity of an attenuated strain (XJCl3) of Junin virus. Intervirology **20:**195–201. http://dx.doi.org/10.1159/000149392.
8. **Kenyon RH, Green DE, Eddy GA, Peters CJ.** 1986. Treatment of Junin virus-infected guinea pigs with immune serum: development of late neurological disease. J Med Virol **20:**207–218. http://dx.doi.org/10.1002/jmv.1890200303.
9. **Enria DA, de Damilano AJ, Briggiler AM, Ambrosio AM, Fernandez NJ, Feuillade MR, Maiztegui JI.** 1985. Late neurologic syndrome in patients with Argentinian hemorrhagic fever treated with immune plasma. Medicina (B Aires) **45:**615–620. (In Spanish.)
10. **Maiztegui JI, Fernandez NJ, de Damilano AJ.** 1979. Efficacy of immune plasma in treatment of Argentine haemorrhagic fever and association between treatment and a late neurological syndrome. Lancet **ii:**1216–1217.
11. **Buchmeier MJ, de la Torre JC, Peters CJ.** 2013. Arenaviridae, p 1283–1303. *In* Knipe DM, Howley PM, Cohen JI, Griffin DE, Lamb RA, Martin MA, Racaniello VR, Roizman B (ed), Fields virology, 6th ed, vol 2. Lippincott Williams & Wilkins, Philadelphia, PA.
12. **Martínez-Sobrido L, Emonet S, Giannakas P, Cubitt B, García-Sastre A, de la Torre JC.** 2009. Identification of amino acid residues critical for the anti-interferon activity of the nucleoprotein of the prototypic arenavirus lymphocytic choriomeningitis virus. J Virol **83:**11330–11340. http://dx.doi.org/10.1128/JVI.00763-09.
13. **Martínez-Sobrido L, Giannakas P, Cubitt B, Garcia-Sastre A, de la Torre JC.** 2007. Differential inhibition of type I interferon induction by arenavirus nucleoproteins. J Virol **81:**12696–12703. http://dx.doi.org/10.1128/JVI.00882-07.
14. **Martínez-Sobrido L, Zuniga EI, Rosario D, Garcia-Sastre A, de la Torre JC.** 2006. Inhibition of the type I interferon response by the nucleoprotein

of the prototypic arenavirus lymphocytic choriomeningitis virus. J Virol **80:**9192–9199. http://dx.doi.org/10.1128/JVI.00555-06.

15. **Eckerle LD, Becker MM, Halpin RA, Li K, Venter E, Lu X, Scherbakova S, Graham RL, Baric RS, Stockwell TB, Spiro DJ, Denison MR.** 2010. Infidelity of SARS-CoV Nsp14-exonuclease mutant virus replication is revealed by complete genome sequencing. PLoS Pathog **6:**e1000896. http://dx.doi.org/10.1371/journal.ppat.1000896.
16. **Qi X, Lan S, Wang W, Schelde LM, Dong H, Wallat GD, Ly H, Liang Y, Dong C.** 2010. Cap binding and immune evasion revealed by Lassa nucleoprotein structure. Nature **468:**779–783. http://dx.doi.org/10.1038/nature09605.
17. **Borden KL, Campbell Dwyer EJ, Salvato MS.** 1998. An arenavirus RING (zinc-binding) protein binds the oncoprotein promyelocyte leukemia protein (PML) and relocates PML nuclear bodies to the cytoplasm. J Virol **72:**758–766.
18. **Djavani M, Rodas J, Lukashevich IS, Horejsh D, Pandolfi PP, Borden KL, Salvato MS.** 2001. Role of the promyelocytic leukemia protein PML in the interferon sensitivity of lymphocytic choriomeningitis virus. J Virol **75:**6204–6208. http://dx.doi.org/10.1128/JVI.75.13.6204-6208.2001.
19. **Campbell Dwyer EJ, Lai H, MacDonald RC, Salvato MS, Borden KL.** 2000. The lymphocytic choriomeningitis virus RING protein Z associates with eukaryotic initiation factor 4E and selectively represses translation in a RING-dependent manner. J Virol **74:**3293–3300. http://dx.doi.org/10.1128/JVI.74.7.3293-3300.2000.
20. **Volpon L, Osborne MJ, Capul AA, de la Torre JC, Borden KLB.** 2010. Structural characterization of the Z RING-eIF4E complex reveals a distinct mode of control for eIF4E. Proc Natl Acad Sci U S A **107:**5441–5446. http://dx.doi.org/10.1073/pnas.0909877107.
21. **Albariño CG, Bird BH, Chakrabarti AK, Dodd KA, Flint M, Bergeron É, White DM, Nichol ST.** 2011. The major determinant of attenuation in mice of the Candid1 vaccine for Argentine hemorrhagic fever is located in the G2 glycoprotein transmembrane domain. J Virol **85:**10404–10408. http://dx.doi.org/10.1128/JVI.00856-11.
22. **Droniou-Bonzom ME, Reignier T, Oldenburg JE, Cox AU, Exline CM, Rathbun JY, Cannon PM.** 2011. Substitutions in the glycoprotein (GP) of the Candid#1 vaccine strain of Junin virus increase dependence on human transferrin receptor 1 for entry and destabilize the metastable conformation of GP. J Virol **85:**13457–13462. http://dx.doi.org/10.1128/JVI.05616-11.
23. **Radoshitzky SR, Abraham J, Spiropoulou CF, Kuhn JH, Nguyen D, Li W, Nagel J, Schmidt PJ, Nunberg JH, Andrews NC, Farzan M, Choe H.** 7 February 2007, posting date. Transferrin receptor 1 is a cellular receptor for New World haemorrhagic fever arenaviruses. Nature **446:**92–96. http://dx.doi.org/10.1038/nature05539.
24. **Flanagan ML, Oldenburg J, Reignier T, Holt N, Hamilton GA, Martin VK, Cannon PM.** 2008. New World clade B arenaviruses can use transferrin receptor 1 (TfR1)-dependent and -independent entry pathways, and glycoproteins from human pathogenic strains are associated with the use of TfR1. J Virol **82:**938–948. http://dx.doi.org/10.1128/JVI.01397-07.
25. **Emonet SF, Seregin AV, Yun NE, Poussard AL, Walker AG, de la Torre JC, Paessler S.** 2011. Rescue from cloned cDNAs and in vivo characterization of recombinant pathogenic Romero and live-attenuated Candid #1 strains of Junin virus, the causative agent of Argentine hemorrhagic fever disease. J Virol **85:**1473–1483. http://dx.doi.org/10.1128/JVI.02102-10.
26. **Pfaffl MW.** 2001. A new mathematical model for relative quantification in real-time RT-PCR. Nucleic Acids Res **29:**e45. http://dx.doi.org/10.1093/nar/29.9.e45.